Characterization and interpretation of select copper occurrences within Banff National Park, Alberta

Permit Number: BANNP-2024-45906 (Multi-HA)

By: Gabriel Johnston, Matthew Smith

May 20, 2025

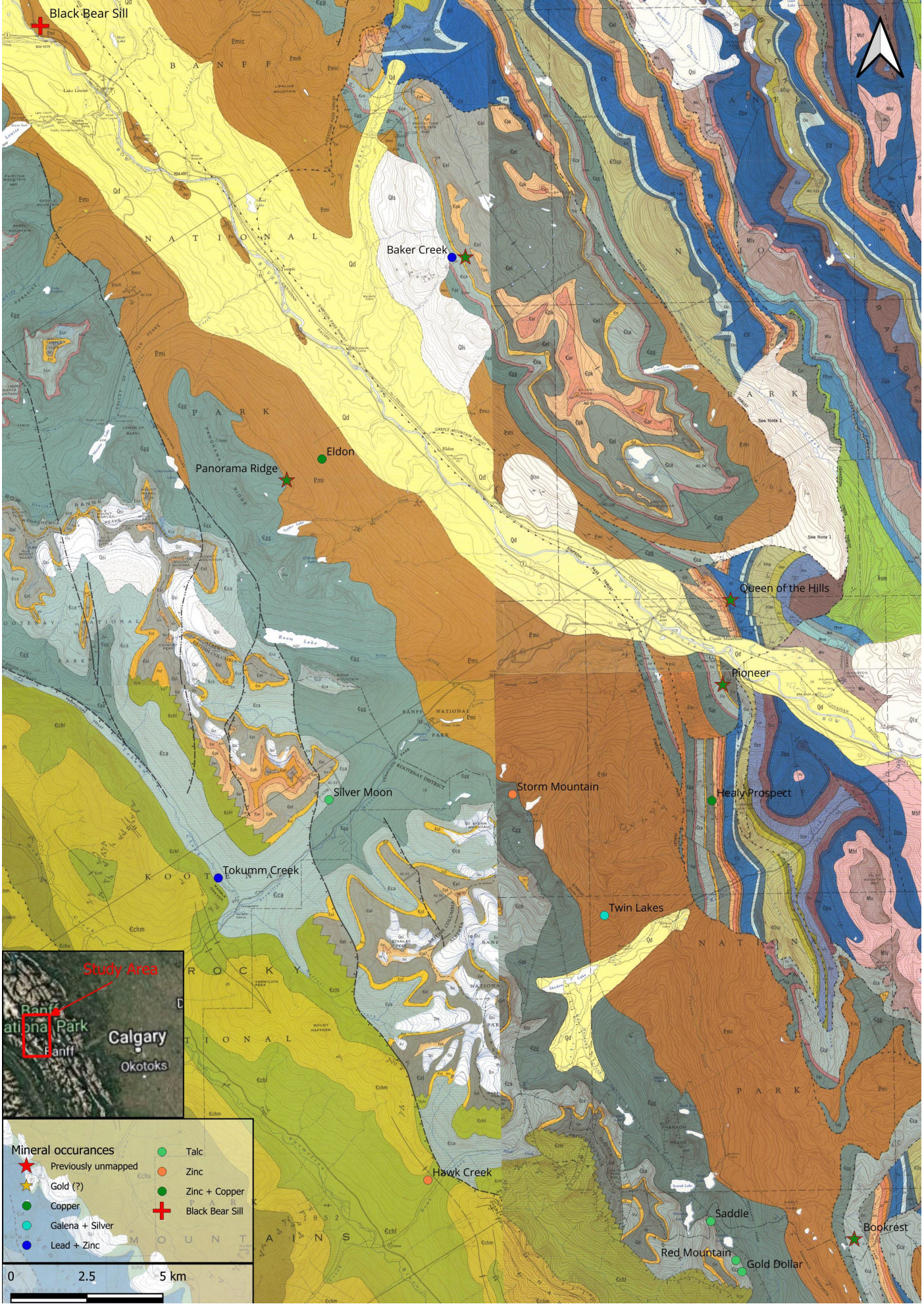

Locations of known mineral occurrences plotted on 1:50000 scale geological map of the area surrounding the BVD. Geological basemaps used, R.A Price Map 1297A, Map 1295A, Map 1476A, Map 1482A. Locations of mineral occurrences provided by BC Minfile database 082N 060, 082N 071, 082N 021, 082O 003, 082O 002, 082O 001, and the Alberta Geological Survey metallic mineral occurrences database, alongside previously unmapped mineral occurrences apparently described for the first time by this report noted by star symbols.

Table of Contents

Introduction:.....4
Geology of the Study Area:.....5
Stratigraphy:.....5
Tectonic History: 6
Methods:.....7
Cu Prospects in the Bow Valley District:.....8
Panorama Ridge Prospect 8
Protection Mountain Prospect 12
Copper Mountain Prospect 15
The Pioneer Prospect.....16
Discussion: 18
Conclusion:.....21
Acknowledgements:.....21
References: 22

Introduction:

Base metal occurrences in Banff National Park, Alberta have historically received limited attention due to their protected status within the park boundary. Nonetheless, understanding the processes responsible for the emplacement of these metallic occurrences will greatly contribute to the geological understanding of the Eastern Canadian Rockies, and may be of importance to understanding multiple metal mineralization occurrences outside of the national park (Mickelsen & Schimdt, 2021; Timmins, 2023; Olson, 1994). Reported in-situ metallic mineralization within Banff National Park includes copper, silver, lead, zinc, and reportedly gold (Hannigan, 1974; Pawlowicz, 2011; Olson, 1994; Roebuck, 1978; Rukhlov, 2011; Allan, 1920; Dawson, 1886; Evans et al, 1965). These occurrences are hosted within the Bow Valley District (BVD), as described by Dawson (1886), and are mostly found within the area surrounding Castle Mountain, AB. The focus of this report is to provide a geological description and comparison of select copper occurrences within the BVD.

The prospects selected for description originally included the Eldon prospect (EP), the Protection Mountain (PM) occurrence, and the Copper Mountain prospect (CM). Following failed attempts to find the EP at the location described by Evans 1965, alongside the discovery of the Panorama Ridge Prospect (PRP). The decision was made to study the PRP in lieu of the EP. Following the completion of 2024 field work, the locations of three other copper prospects were brought to the attention of the authors. These included the Copper Mountain "Pioneer" prospect, the Queen of the Hills prospect, and the Bookrest prospect. Of these prospects, only the Pioneer prospect was observed and characterized via field observations for this report, however due to the Pioneer prospect being located outside of the outlined 2024 research and collection permit study areas, no samples were collected. The coordinates of the latter two prospects are known and have been plotted on this report's geological map of the area.

Three distinct styles of copper mineralization have been observed within the BVD, suggesting multiple episodes of copper-mineralizing fluid flow. The most common style is dominantly quartz vein-hosted Cu mineralization within Middle Cambrian carbonate units, primarily the dolomitized Eldon Formation, as seen at the PM and CM prospects. The second type is the quartz vein-hosted Cu-Zn mineralization within late Proterozoic siliciclastic units, as described at the EP (Evans et al, 1965). The third type is the calcite vein-hosted Cu-Ag mineralization within the late Proterozoic Miette Group, as seen at the PRP. Both the EP and PRP are hosted within the Neoproterozoic Miette Group, however, due to differences in their vein composition and mineralization they are interpreted to represent separate phases of mineralization. Due to the vein hosted nature of the BVD Cu mineralization, the deposit models of these occurrences are unlikely to fall under the models of either the Kipushi type (Bernstein, 1992) or Stratiform Sediment-hosted Cu type deposits (Cox, 1992), as could be expected for these occurrences which are of unknown origin and lack clear evidence of igneous connection. Instead, as suggested by Evans et al (1965), Hannigan (1974), and this report, these copper occurrences may represent true vein type styles of mineralization, possibly of mesothermal origin such as that found at the Coeur d'Alene mining district in Idaho.

The geological descriptions of the prospects will be built upon data collected from field and laboratory data. Collected data alongside previous reports will be used for the geological comparison of the BVD Cu prospects. This paper provides the first known age constraint on copper mineralization within the BVD, particularly that of the PRP, using relative age dating methods. Furthermore, this paper will then attempt to establish the controls on ore mineralization and attempt to recognize a deposit model most suitable to the BVD Cu mineralization.

Geology of the Study Area:

Stratigraphy:

The BVD is composed mostly of Neoproterozoic to upper Cambrian strata, alongside Ordovician and Devonian strata, although there is no recorded metallic mineralization within post-Cambrian units. Detailed descriptions of stratigraphic units in the study area exist (Aitken, 1997; Aitken, 1969), this report provides a concise overview of Proterozoic to Late Cambrian strata, arranged chronologically.

Miette Group Within the study area the Miette Gp is split into two formations, the upper Hector Formation and the lower Corral Creek Formation. The Hector Fm is defined as a dominantly shale unit characterized by red, green, and purple colors (Aitken, 1969). Near Lake Louise (nearby this project's study area), the Hector Fm is known to contain beds of conglomerates with varying thicknesses. This includes all Precambrian grits, interbedded slates, and conglomerates overlaying the Walcott type Hector Fm of Redoubt Mountain (Aitken, 1969). The Hector Fm overlies the Corral Creek Fm, which is defined by gray and greenish slates and some siltstone beds, which are interbedded with variable amounts of grits, and quartz pebble conglomerates indistinguishable from those assigned to the upper Hector Fm (Aitken, 1969). Therefore, the division of the Hector and Corral Creek Fm's can only be made with recognition of the purple and green slates associated with limestone bearing conglomerates (Aitken, 1969).

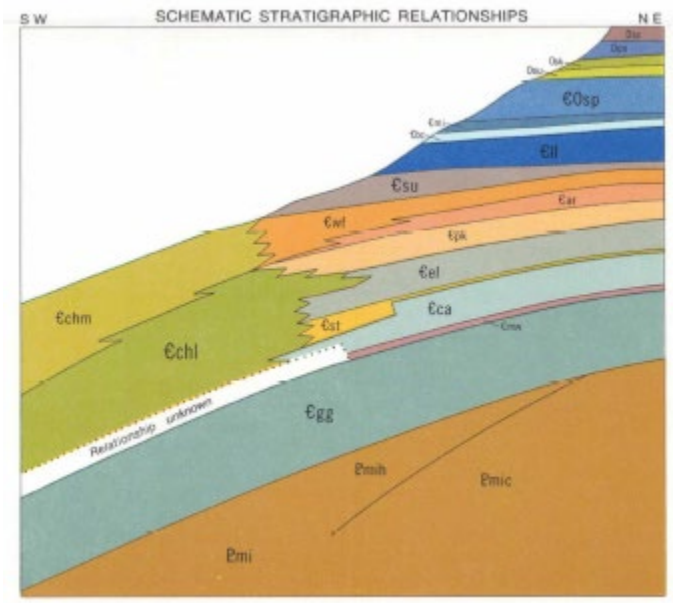

Figure 1: Schematic stratigraphic relationships of the strata within the study area (Price, 1975 – Map1482A).

Gog Group: The Gog Gp contains five distinguishable units, the Jasper Fm, Fort Mountain Fm, Lake Louise Fm, St. Piran Fm, and Peyto Fm. The Gog Gp is dominated by siliciclastic units, however the upper most Peyto Fm is recognized by its locally dolomitized resistant limestone. Notably the Jasper Fm of nearby Redoubt Mountain is only 0.5 m thick, and absent at Castle Mountain. Furthermore, at Castle Mtn the St. Piran Fm pinches out and the entire Gog Gp appears thinner which may represent syndepositional rifting (Desjardins, 2010).

Mount Whyte Formation: Recessively weathering unit of shale, siltstone, and minor sandstone which unconformably overlies the Peyto Fm within the study area (Aitken, 1997).

Cathedral Formation: The lower of the two main Middle Cambrian dolomite and limestone cliff forming formations. Contains two shaley tongues, the lower Ross Lake Shale Member and the upper Trinity Lakes Member (Aitken, 1997).

Stephen Formation: Recessive-weathering unit of greenish shale with beds of limestone separating the thick carbonate packages of the Cathedral Fm and Eldon Fm (Aitken, 1997).

Eldon Formation: The upper most of the two main Middle Cambrian cliff forming formations. At the Castle Mountain type section, the Eldon Fm forms steep slopes and cliffs and has been dolomitized (Aitken, 1997).

Pika Formation: Composed of well-bedded carbonate rocks interrupted by the lower units of shale. The Pika is darker than the Eldon, the lower Pika is relatively recessive compared to the more massive Eldon Fm (Aitken, 1997; Slind, 2025).

Arctomys Formation: Recessive interval of brightly red coloured shales and subordinate carbonates between the Pika Fm and the Waterfowl Fm. There is evidence to suggest evaporites were once present (Slind, 2025).

Waterfowl Formation: Resistant, cliff forming carbonate and siltstone unit gradationally overlying the Arctomys Fm. Characteristically defined by stylolites, beds of oolites and stromatolites (Slind, 2025).

Sullivan Formation: A recessive interval of greenish-gray and brown shales interbedded with thin limestone layers. Sharply overlies the Waterfowl Fm and gradationally transitions to the Lyell Fm (Slind, 2025).

Lyell Formation: Massive, cliff forming carbonate unit (Slind, 2025).

Tectonic History:

1) ***Rifting, fragmentation, and separation of the supercontinent Rodinia by the Neoproterozoic (~750Ma):*** As continental fragments separated, an oceanic basin formed along the ancient western margin of Laurentia (Ancient North America). This stage is recorded by the lower portion of the Windermere Supergroup (Price, 2002). Rifting has been interpreted to have continued during the Lower Cambrian deposition of the Jasper Fm (Desjardins, 2010), and possibly reactivated in the Middle Cambrian, represented by the Kicking Horse escarpment (McCormick, 2024).
2) ***Transition from rifting and seafloor-spreading to a miogeoclinal/ passive margin:*** setting along the western margin of Laurentia occurred ~545 Ma or as late as 488 Ma (McCormick, 2024).
3) ***The Passive margin***: the passive western margin of Laurentia continued until the Middle Devonian (~390 Ma). The end of the passive margin is marked by the onset of arc magmatism on the Laurentia plate margin (Price, 2002). Within the passive margin timeframe, reactivation of the passive margin has been interpreted in areas directly westward of the study area. Following the end of the passive margin is the Late Devonian to Early Carboniferous Slide Mountain back arc basin extension, which has been suggested as responsible for normal fault creation near the study area and the formation of the Igneous Ice River Complex (Taerum, 2022; Mumford, 2009).
4) ***Contractional deformation:*** of the study area occurred in two main pulses (Pluijm, 2014; Evenchick, 2007). The first major pulse within the study area (represented by the Simpson Pass thrust fault) was the Jurassic-Cretaceous fold-thrust belt (the Cordilleran Orogeny), which was followed by the more pronounced Late Cretaceous-Eocene fold-thrust belt deformation, responsible for carrying the previously deformed fold-thrust belt eastward (the Laramide Orogeny) (Evenchick, 2007; Pluijm, 2014). Deformation of the Rocky Mountain fold and thrust belt accommodated up to 200 km of horizontal shortening (Bally, 1966; Price, 1981; Price, 1985; Fermor, 1992).
5) ***Post orogenic extension:*** from the Late Paleocene to Eocene. Normal faults in the area have been interpreted to have resulted from post orogenic, transtension-extension west of the Rocky Mountain Trench. Locally this extension has exposed Omineca Belt metamorphic rocks from depths of >25 km (Price, 2002; Taerum, 2022).

Methods:

The data used within this report is sourced from both field and laboratory work. Field work was conducted over a week in early September 2024. Work focused on finding and describing the nearby Protection Mountain (Baker Creek), Copper Mountain, and the Eldon prospects as outlined in the research collection permit provided by Banff and Yoho National Parks. The field crew was composed of both authors. Daily excursions were conducted from a basecamp located at Tunnel Mountain Campground, near the townsite of Banff, AB. Excursions involved driving to hiking access points, from which the field crew hiked to the prospects. Following creeks and trails when able. Some sites, particularly the Copper Mountain prospect lacked trails and involved significant route finding through dense brush. All field days involved ~20km traverses to study areas. Permitted study areas were predefined using literature research alongside previously mapped locations of Cu occurrences indicated by the Alberta Energy Regulator (AER). The previously unmapped or referenced PRP was accidentally found while the field crew was enroute to find the Eldon prospect. However, the Eldon prospect was not found at the location described by Evans et al, 1967. Following this initial work, in late September the authors supervising professor Dr. Paul Johnston, and MRU adjunct professor Dr. Chris Collom joined two daytrips to BVD prospects (PRP, and PM), assisting with geological interpretation and providing mentorship.

A Garmin GPSMAP 66i GPS device was used for navigation and recording of GPS coordinates of field stations, samples, and geological structures. All sampling was completed with rock hammers, chisels and a geotool. Sample ID followed the format of (Study Area Name) -(Sample#) – (If multiple samples collected from same location, second sample #) - (Year of Sample) - (name of sampler), an example of this is (Ed-1 - 24-GJ), this represents the first sample collected from the Eldon prospect study area in 2024 and the sampler is Gabriel Johnston.

Field notes and observations were recorded in notebooks and later digitized using geospatial software QGIS and Google Earth Pro. Field work consisted of exploration, mapping, composing geological descriptions of lithologies and geological features encountered in the field.

Alongside field work, petrographic analysis was conducted via thin sections prepared on and off campus, and geochemical analysis was conducted by Kamloops Activation Laboratories. Geochemical data was derived by Multi-Method Analyses, involving both ICP-MS and INAA analysis of whole rock samples collected during field work. Petrographic analysis involved petrographic descriptions of host rock, microstructures, and ore petrography from both transparent thin and reflected thick sections. 30 thin sections, 7 polished thick sections, and 5 sections prepared for fluid inclusion were used.

Cu Prospects in the Bow Valley District:

Panorama Ridge Prospect

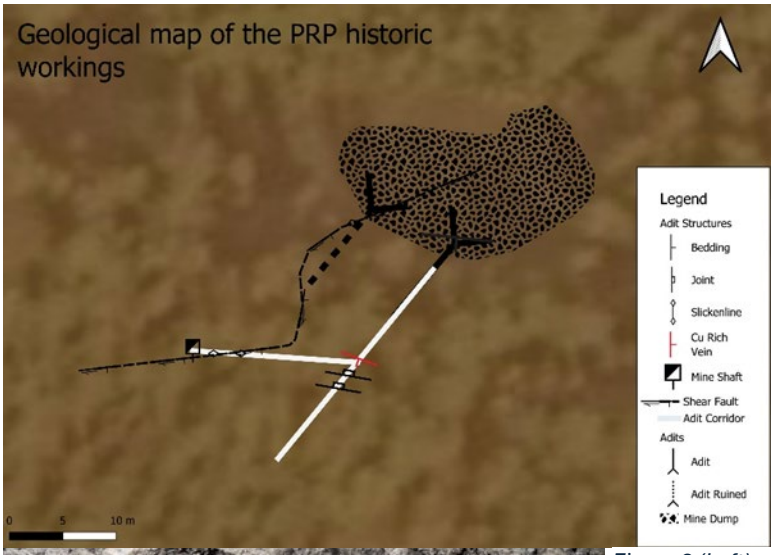

Figure 3 (Left): The Cu vein as mapped in Figure 2 (Above). The Cu vein pinches and swells along the length of a fault ~7cm wide, with the same trend as the Cu vein. Note: the shattered metapelites below the ore vein.

The Panorama Ridge prospect is situated on the North easternmost spur of Panorama Ridge. Metallic mineralization primarily consists of chalcocite, covellite, bornite, minor amounts of chalcopyrite, and silver. Gangue mineralization consists of calcite, siderite, and barite. Metallic mineralization is both hosted within carbonate veins and as blebs within the slate wall rock. Known historical development of the PRP consisted of two adits and a prospect pit ~800 meters NW of the adits. Judging by the material present in the dump downslope of both adits and the length of the adit still accessible, it appears the adits of the PRP were driven further than that of the much better described CMP, although no information could be found concerning the PRP history. To the author's knowledge, this is the first geological report on the PRP.

Cu mineralization of the PRP is hosted within the green, purple, and brown slates characteristic of the lower Hector Fm, however, the Hector Fm host rock is uncertain due to the inability to recognize basal Hector Fm limestone conglomerate beds. Slates grade upwards into grey beds of grits and gently dip (150 / 25). Unconformably overlying the Miette Gp is the Lower Cambrian Fort Mountain Fm, identified as the cliff-forming, massive, purplish quartzite sandstone unit ~20 meters upslope from both observed Cu occurrences of the PRP.

Host Rock: The host rock mineral assemblage identified by petrographic analysis of the country rock is quartz, calcite, siderite, chlorite, muscovite, and albite. The lateral equivalent to the Hector Fm is the Old Fort Point Fm, the metamorphic assemblage of the Old Fort Point Fm has been interpreted to have formed at temperature–pressure conditions of ~300°C and 8 Kbars (Charlesworth, 1967), and has been age-dated to be younger than 75 Ma using K/Ar radiometric age measurements of micas presumably formed during metamorphism (Charlesworth, 1967). Due to similarity of the host rock mineral assemblage and the description of the Old Fort Point Fm by Charlesworth, (1967) the same metamorphic pressure–temperature conditions and age have been assumed for the PRP study area.

Geological Structures: Structures observed and measured at the PRP consist of faults, foliations, and veins. Three faults were identified in the immediate vicinity surrounding the PRP adits. Two of which appear to be a set of strike slip faults with near horizontal movement, as indicated by slicken lines. This fault set crosses the upper collapsed adit (080/64) and is seen again within the adit near the vertical mineshaft (064/45). The third observed fault runs approximately (110/26) and hosts the slightly boudinaged ore bearing carbonate vein. There are two foliation fabrics observed at the PRP, the first of which is the dominant bedding parallel fabric (S1) likely to be associated with regional Paleozoic burial. The second observed fabric is non pervasive crenulation cleavage (S2) associated with the deformation of barren quartz veins.

Veins: Two distinct sets of veins are observed at the PRP. Due to the deformed nature of the extensional barren quartz veins (V1) and the S2 fabric, V1 has been interpreted to represent the first known stage of fluid flow, occurring under normal stresses as suggest by vein quartz growth perpendicular to the vein walls. The width of V1 varies from ~3 -1cm. No significant alteration has been observed to be associated with V1. Following V1 is the ore mineralizing fluid flow associated with relatively undeformed (compared to V1) carbonate veins, V2 crosscuts both S1, S2 and V1. Alteration salvages of calcite flooding vein walls are clearly associated with thicker V2 veins. The width of V2 varies significantly from >5cm to veinlets (~1mm) thick. Both the boudinage, association with nearby faults, and calcite deformation twins of the V2 suggest continued compressional stress although not as significant as the deformation responsible for the deformation of V1.

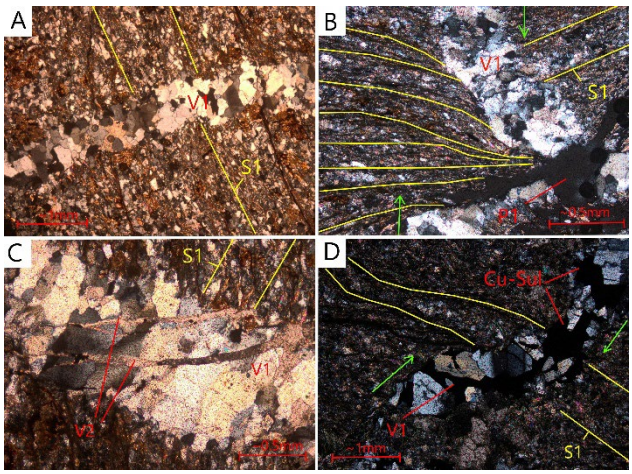

Figure 4: Thin sections in Polarized light containing V1. (A) V1 crosscuts S1 fabric, XPL 5x magnification. (B) Buckling of V1 and the deformation of S1 fabric. Green arrows represent σ1 stress deforming V1 and S1. P1 represents unfilled secondary porosity induced by the deformation of V1. XPL 5x magnification (C) V2 calcite veinlets cross cutting V1. XPL 10x magnification (D) Porosity induced by the deformation of V1, Induced porosity hosts Cu-Sulphides. S1 rotation mirrors rotation of V1. XPL 5x magnification.

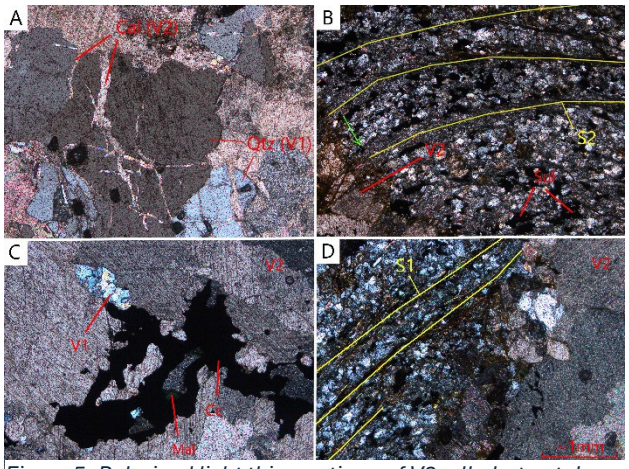

Figure 5: Polarized light thin sections of V2, all photos taken in 5x magnification. (A) V2 filling and supporting a fractured V1 fragment. (B) V2 truncates S2. Note: Sulphides (Sul) in country rock do not follow S1 fabric. (C) Chalcocite (Cc) hosted by V2, Malachite (Mal) forming on Cc margins. Note: Clast of V1 supported by V2, and deformation twins of Calcite (Cal). (D) S1 fabric truncated by V2.

Ore Petrography:

Ore minerals identified at the PRP are chalcocite (Cu2S), covellite (CuS), bornite (Cu5FeS4), and chalcopyrite (CuFeS2). Both bornite and chalcopyrite are intimately associated. Chalcopyrite is present as exsolution within bornite displaying basket weave textures, and blades of chalcopyrite within chalcocite and bornite. The basket weave texture suggests the replacement of chalcopyrite by bornite (Kan Li, 2018).Therefore, chalcopyrite likely represents the primary hypogene ore mineralization, followed by bornite replacement of

chalcopyrite , and subsequent in-situ oxidation of chalcopyrite and bornite to chalcocite and then covellite with a paragenesis sequence as such: chalcopyrite → bornite → chalcocite → covellite.

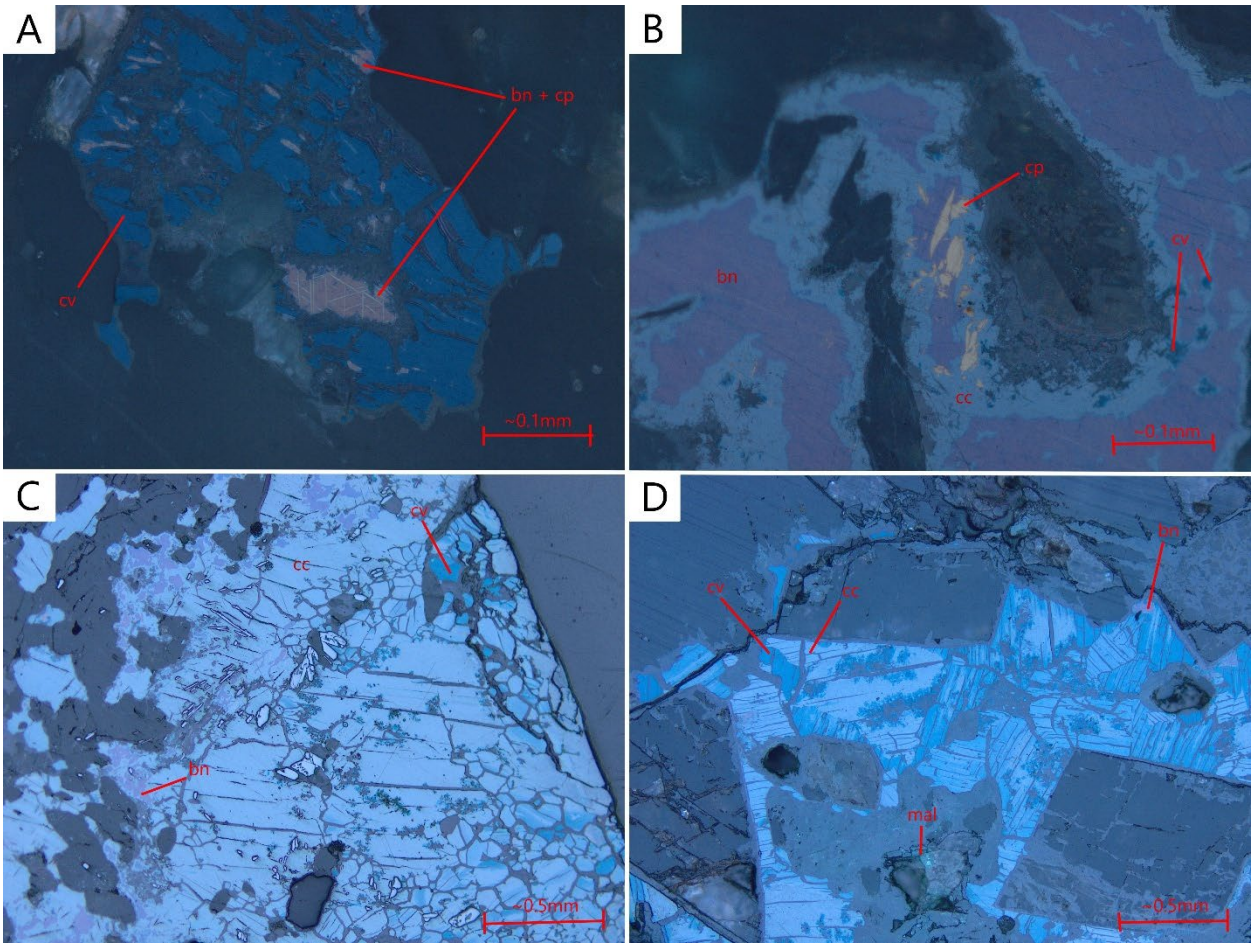

Figure 6: Reflected light thin sections prepared from samples taken from the PRP adits. (A) Thin section Ed-3-5-24: Bornite (bn) with chalcopyrite (cp) exsolution displaying basket weaving texture indicative of bornite replacement of chalcopyrite. Note the replacement of bornite by covellite (cv). (B) Thin section Ed-3-5-24 Primary bornite and chalcopyrite has been replaced by chalcocite (cc), which itself is partially replaced by covellite. (C) Thin section Ed-3-3-24 bornite has been replaced by chalcocite, note the parallel fractures produced by volume loss associated with the chalcocite replacement of bornite. Chalcocite is partially replaced by covellite along fractures and grain boundaries. (D) Thin section Ed-3-3-24: Chalcocite partially replaced by covellite along fractures and grain boundaries, trace amounts of bornite still remain after chalcocite alteration.

Geochemistry:

Multimethod geochemical analysis by Act Labs Kamloops was conducted on five whole rock grab samples. The results of the geochemical analysis have been attached at the end of this report. Portable XRF data was also collected, however the results of whole rock analysis provided completely different values for certain elements. The portable XRF data was then regarded as unreliable and thus the data is not referenced.

Samples taken from the adits mine dump (Ed-3-24-GJ, Ed-5-24-GJ) yielded anomalously high concentrations of both Cu (>1%) and Ag (136, 61ppm) with comparatively low concentrations of Pb and Zn. As shown in table 1, most metallic minerals are highly correlated except for Zn which is very poorly correlated with other ore minerals. Ore bearing samples also contained trace amounts of Mo, Co, Cr, Ni. PRP Cu bearing veins have characteristically high Ba content (3-5%) and relatively high concentrations of rare earth elements (ΣREE =

~86 ppm). Notably, sample Ed-4-3-24-GJ collected to serve as an unmineralized base line of the nearby Miette Gp contained anomalous concentrations of Cu (3060 ppm).

Trace Elements: Due to the dominantly carbonate composition of V2, rare earth elements + yttrium (REEY) signatures can be used to help define the source rock of the ore bearing veins using a source-sink system approach (Debruyne, 2016). Source inherited REEY characteristics can be induced by patterns of REEY spyder diagrams. REEY spyder diagrams produced from the carbonate ore bearing veins of PRP do not align nicely with typical patterns of meteoric, sea water, or magmatic water, suggesting significant fluid rock interaction (Debruyne, 2016). Usually, it is not possible to trace REEY values back to their sources, except for Eu anomalies in low temperature systems (<250°C) and sometimes Y/Ho values (Debruyne, 2016). In lieu of this, an Eu/Eu_{N^*} value calculated from V2 REEY concentrations is 0.45, suggesting that the V2 Eu/Eu_{N^*} signature may be inherited from a magmatic source. However, fluid inclusion work is needed to confirm that the veins precipitated at temperatures lower than 250°C, allowing for reliable Eu/Eu* interpretation (Debruyne, 2016). The Y/Ho_N ratio calculated from V2 concentrations is ~1.3 which could indicate reservoir inherited features from either a seawater or a magmatic reservoir. Ce/Ce_N^* calculated using equation 2 indicates an Ce/Ce* ratio of 0.86, which may represent features inherited from a magmatic, anoxic or oxic seawater reservoir (Debruyne, 2016).

$$Equation\ 1: \frac{Eu_N}{0.5(Sm_N+Gd_N)} = \frac{Eu_N}{Eu_{N^*}} \qquad Equation\ 2: \frac{Ce_N}{Ce_{N^*}} = \frac{Ce_N}{0.5(La_N+Pr_N)}$$

	Ag	Cu	Mo	Pb	Zn
Ag		0.876163	0.969362	0.853523	-0.04807
Cu	0.876163		0.738046	0.849686	0.217327
Mo	0.969362	0.738046		0.739118	-0.10048
Pb	0.853523	0.849686	0.739118		-0.3161
Zn	-0.04807	0.217327	0.217327	-0.3161	

Table 1: Correlation matrix of selected metals from the PRP. Note, the extremely low correlation between Zn and other metals.

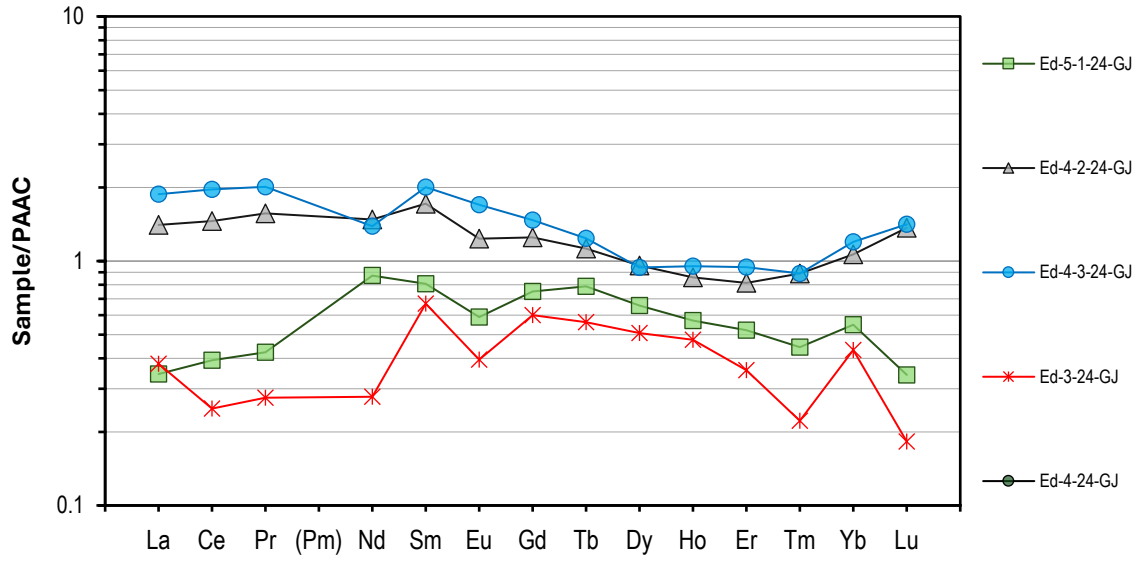

Table 2: PAAC (Pourmand, 2012) normalized REE concentrations from the PRP. Note the depleted Eu anomaly of the ore bearing carbonate veins (V2).

Protection Mountain Prospect

The Protection Mountain (PM) occurrence is located on the southern slope of Protection Mountain, found immediately northwest of Castle Mountain. Copper mineralization is the primary type of metallic mineralization observed during field work, while previous reports of nearby lead or zinc at the Baker Creek prospect could not be confirmed (Evans et al, 1965; Hannigan, 1974). The copper mineralization occurrence had been known during the 1880s, as noted by George Dawson on the map associated with his 1886 preliminary report of this area and was previously explored, as indicated by the presence of a prospect pit found at the base of a copper mineralized quartz vein. However, the age of this working is not known. Metallic mineralization found in the Protection Mountain occurrence dominantly includes chalcocite and, lesser quantities of covellite and chalcopyrite. Gangue minerals associated with the ore minerals include abundant goethite, hematite, quartz, and dolomite.

Host Rock:

The copper mineralization is hosted within the Eldon Fm, a well-bedded, dolomitized limestone unit. This overlies the shale Stephen Fm, which in turn overlies the massive limestone Cathedral Fm which hosts the MVT lead—zinc Baker Creek prospect.

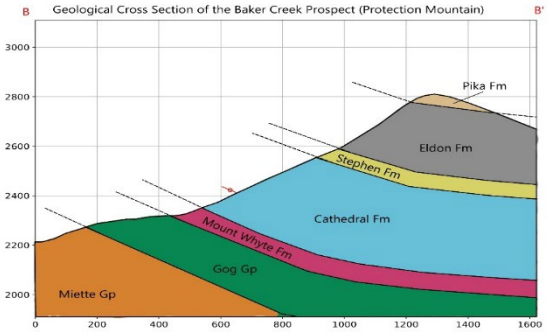

Figure 7: Geologic cross section (B-B') from the map of the Baker Creek prospect.

Figure 8: (A) Cataclasite carbonate leached (?) matrix with larger brecciated fragments of dolomite host rock, contains blebs of chalcopyrite within the matrix. (B) Cu mineralized quartz stringers forming around dolomite breccia fragments within a dolomite dissolution breccia. (C) Milky white massive quartz vein with patchy malachite mineralization, Matthew Smith standing for scale.

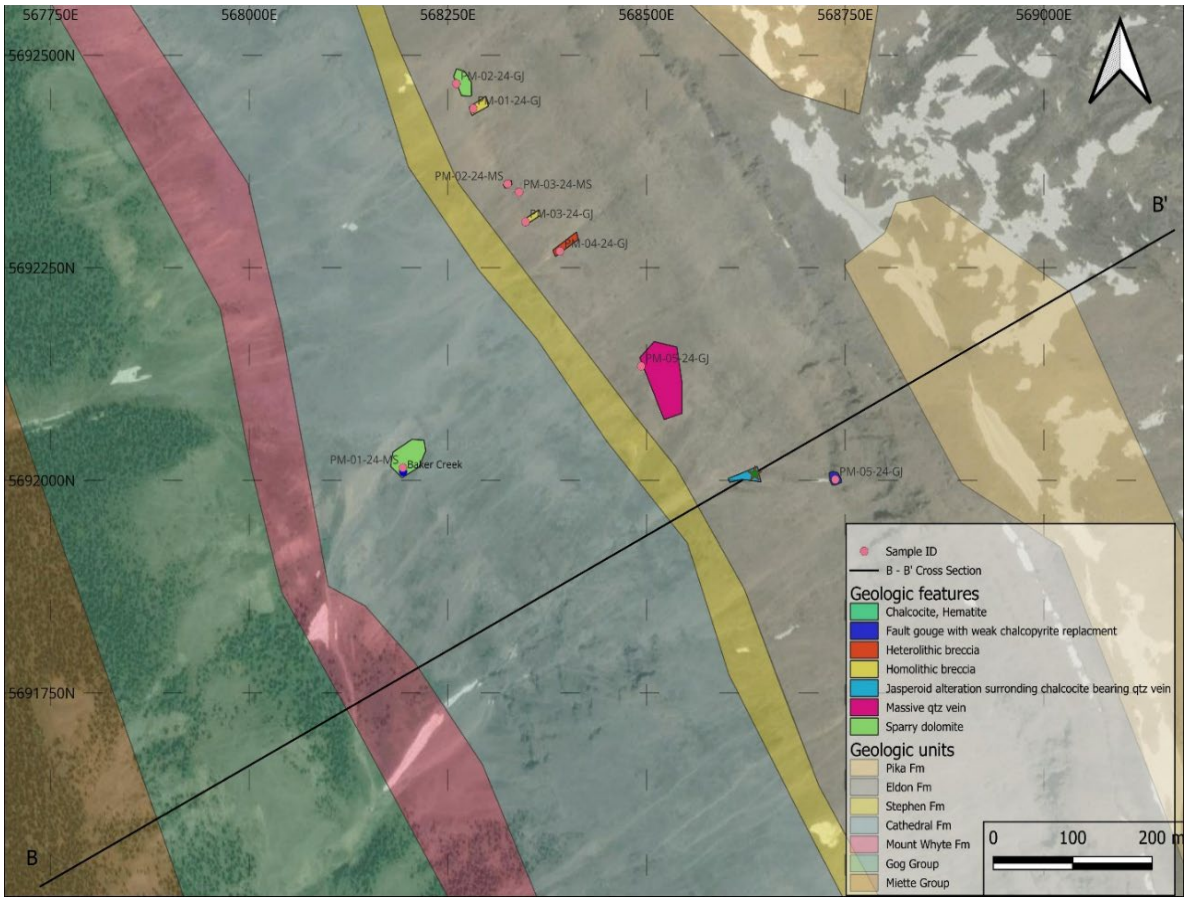

Figure 9: Geological features and sample locations at the Baker Creek prospect. Bedrock geology was digitized after Map 1482A.

Veins and Structures: The Protection Mountain occurrence features several veins and fault styles. Veining within the study area includes sparry dolomite vein stockworks, although associated with reported lead – zinc MVT style of mineralization and does not appear associated with copper ore mineralization apart from trace amounts of malachite. Copper ore mineralization instead is restricted to quartz veinlets, dolomite breccias with quartz vein matrix, an massive milky white quartz vein, and a fault-controlled quartz vein running approximately perpendicular to jasperoid altered country rock. The proximity of quartz matrix dolomite breccias and sparry dolomite matrix dolomite breccias, suggest that the later cupriferous silica rich fluids may have reused the dolomite breccias as conduits for fluid flow. Jasperoid alteration is observed immediately surrounding a brecciated copper bearing quartz vein, suggesting low PH and mean homogenization temperatures of ~200°C of silica rich cupriferous fluids.

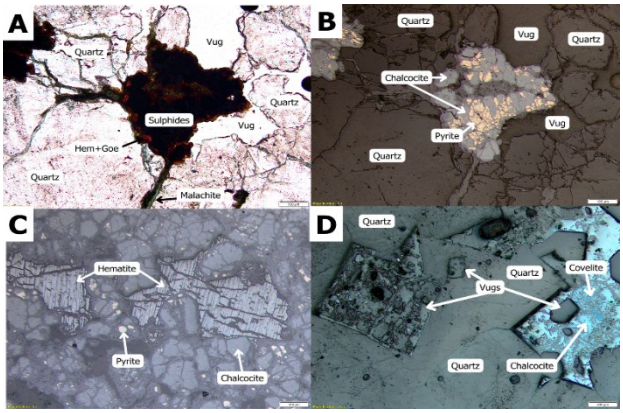

Figure 10: (A) Thin section PM-02-24-MS in PPL, showing a vuggy quartz veinlet with sulphide mineralization with iron oxide mineralization surrounding the vug and filling nearby fractures. (B) Thin section PM-02-24-MS in reflected light, showing chalcocite replacement of pyrite. (C) Thin Section PM-18-24-MS, hematite filling spaces between pyrite replaced by chalcocite. (D) PM-05-24-MS in reflected light, chalcocite partially replaced by covellite. Chalcocite appears to have completely replaced pyrite in this section.

Petrography:

Observed ore mineralization at PM consists of chalcopyrite, chalcocite, covellite, malachite, azurite, with gangue minerals of quartz, dolomite (both sparry veins and grey dolomite wall rock), and ankerite. Jasperoid alteration is observed at a fault-controlled copper mineralized quartz vein, indicative of a low Ph fluid system with mean homogenization temperatures of ~200°C (Lovering, 1962). Observed replacement of pyrite by chalcocite may indicate an oxidizing ore forming environment under significant influence of supergene enrichment processes. Interestingly, chalcopyrite (a common hypogene mineral and not commonly formed by supergene enrichment, and not vein hosted) is found in-situ within cataclasite rock found above the jasperoid altered vein and other occurrences of chalcocite.

Geochemistry:

Geochemical analysis of the PM occurrence indicates an notable disparity between the concentrations of Cu and those of Zn and Pb. Fe concentrations remain relatively high along with the high Cu concentrations, as is reflected in the mineralogy of the PM occurrence. Furthermore, the quartz veins contained no appreciable amounts of REEY and minor concentrations of Ag. No Au was detected within any PM samples.

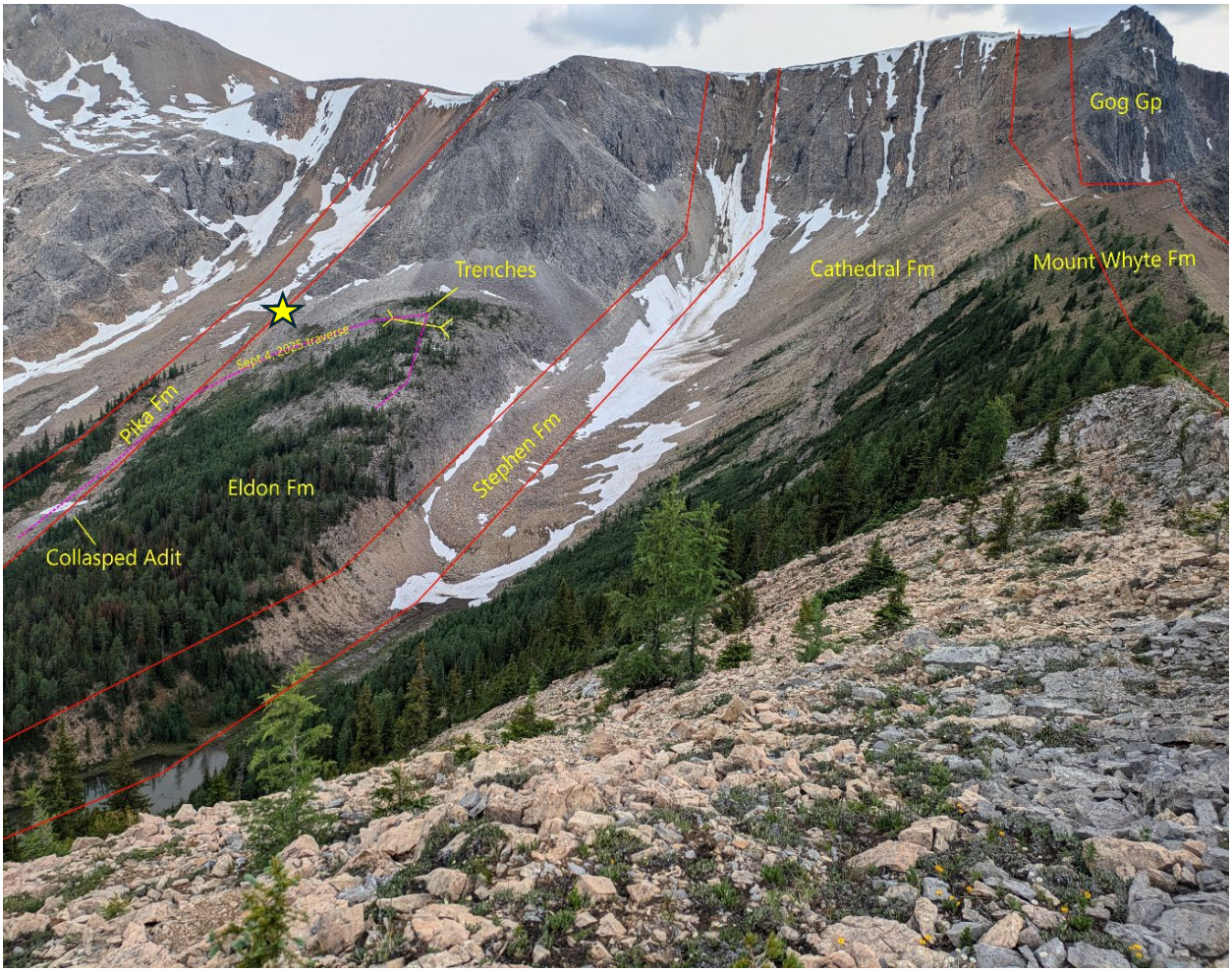

Figure 11: Looking down on the Copper Mountain cirque containing the Copper Mountain prospect. Note the geological units, and the locations of observed historical development. The September 4, 2025 traverse marked by the purple hashed line. The yellow star marks the approximate area which Mr. Nylund found the Cu mineralized talus.

Copper Mountain Prospect

Copper Mountain Cu mineralization is restricted to the nearly vertically dipping Eldon Fm (bedding 178/74) and occurs at multiple sites along its exposure. The mineralization resembles that of the PM. The CM likely received the highest degree of development and is the best documented occurrence within the BVD. Historical development of the prospect included an adit ~60 meters (the Alberta Mine), several prospect pits, alongside multiple buildings meant to support the exploration, including a blacksmith shop (Dennis, 1887). Notably, no Cu ore mineralization was found within the mine dump of the collapsed Alberta Mine.

Host Rock:

Cu mineralization is constrained within the thick bedded dolomitized Mid Cambrian Eldon Fm.

Geological Structures:

No significant geological structures were observed. However, bedding of the host rock has been overturned and dips nearly vertical.

Veins:

Although multiple Cu occurrences are reported at the CM (Dawson, 1885), only the previously described (Dawson, 1885) trenched-out quartzite vein was observed during field work by this papers author to host in-situ Cu mineralization, albeit only copper oxides. Furthermore, azurite and malachite were noticed within blocks of breccia dolomite (very similar characteristically to the PM dissolution breccia) found within the talus. Significant quartz vein hosted Cu mineralization was found in talus below the east side of the spur which the field crew had traversed up (C.Nylund, personal communication) (this was brought to the attention of the authors after field work had been completed).

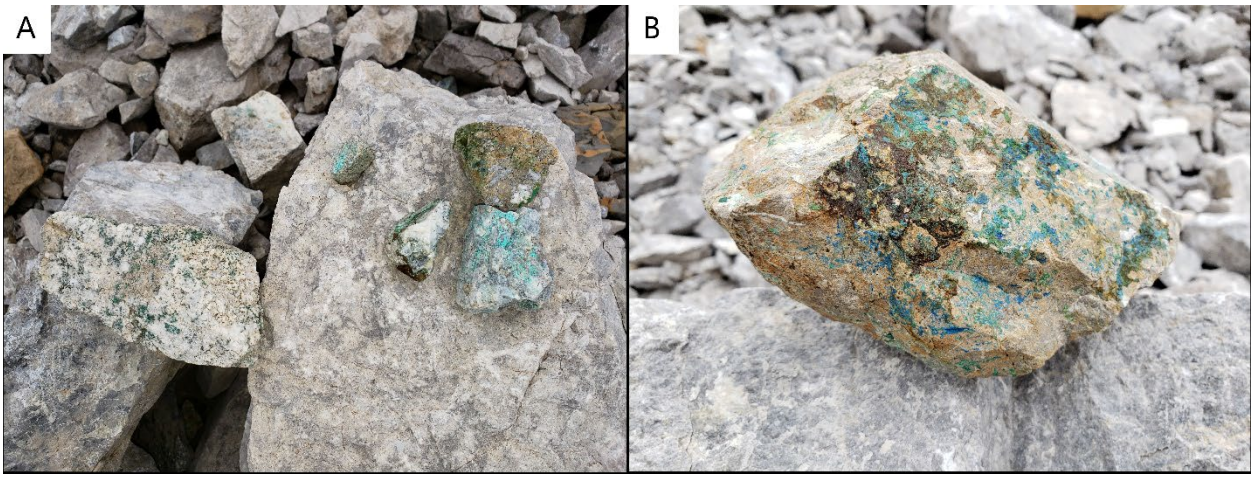

Figure 22: Photos by C.Nylund

Due to previous work on the quartzite vein, reliable measurements could not be taken from the vein. The orientation of the trench alongside historic descriptions (Dawson, 1885) suggests an orientation of (090/80). Notably this quartz altered carbonate rock from the Copper Mountain prospect is coarser grained then the vein related jasperoid alteration found at the PM. However, they are likely related due to their relationships to Cu mineralization and their similar orientations (after the bedding of copper mountain is rotated to the same bedding plane as Protection Mountain) within the same host formation (Eldon Fm).

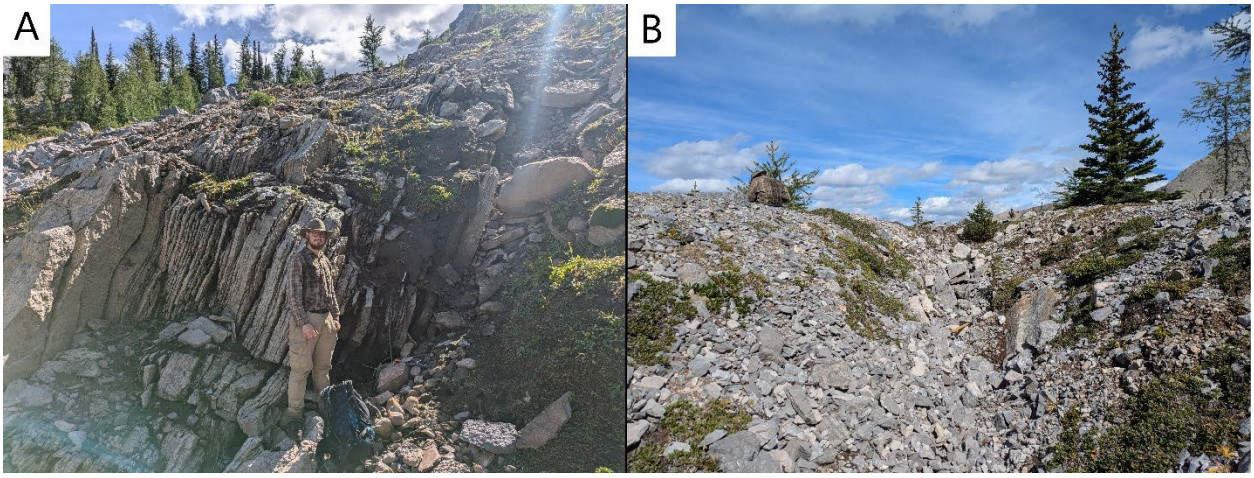

Figure 13: (A) Matthew Smith standing next to the collapsed Copper Mountain prospect (Alberta Mine) adit portal. (B) Historical trench workings of the Cu mineralized quartzite vein. Note: Dissolution dolomite breccia with faint patches of Cu carbonates were found in the talus nearby the trenches.

The Pioneer Prospect

Similar to the PRP, the Pioneer prospect (PP) has no prior geological description. To the authors' knowledge, this report provides the first geological characterization of the PP. However, due to the location of the PP outside the permitted collection areas, no samples were collected, and only field observations could be made. The PP is situated on the northern foot of Copper Mountain, ~700 meters from highway 1. Historical documentation of the PP is poor, and the only known reference is a map produced concerning mineral claims on Copper Mountain (Dennis, 1887). Known historical development of the PP includes two adits driven ~10 meters each, and a prospect pit located upslope of the adits. Cu mineralization is documented at three locations: i) chalcocite hosted within lower quartz veinlet stockworks, ii) Cu carbonates and sulfides in the quartz – carbonate vein stockwork targeted by the adits, iii) azurite and malachite at the upper prospect pit. The reasoning for the cease of work is unknown as abundant copper mineralization is found at the end of the easternmost adit.

Host Rock:

Observed mineralization at the PP is limited to the Eldon Fm.

Structures:

Unlike the CM and PM, mineralization at the PP is significantly controlled by faulting, the abundant vein stockworks likely representing a fault zone, and the abundance of unhealed fractures representing post mineralization seismic activity. The lowermost copper occurrence is hosted within a dilation jog filled with blebby chalcocite and fragments of dolomite wall rock within vein quartz, indicating dextral sense of shear movement (172°-352°). Both adits target an extensively fractured Cu mineralized quartz - carbonate vein stockwork, and multiple unmineralized faults crosscut the ore bearing vein stockwork. Slicken lines indicate a dominantly high angle upward sense of movement of the hanging walls, indicating a compression stress regime possibly associated with the nearby Johnston Creek Thrust.

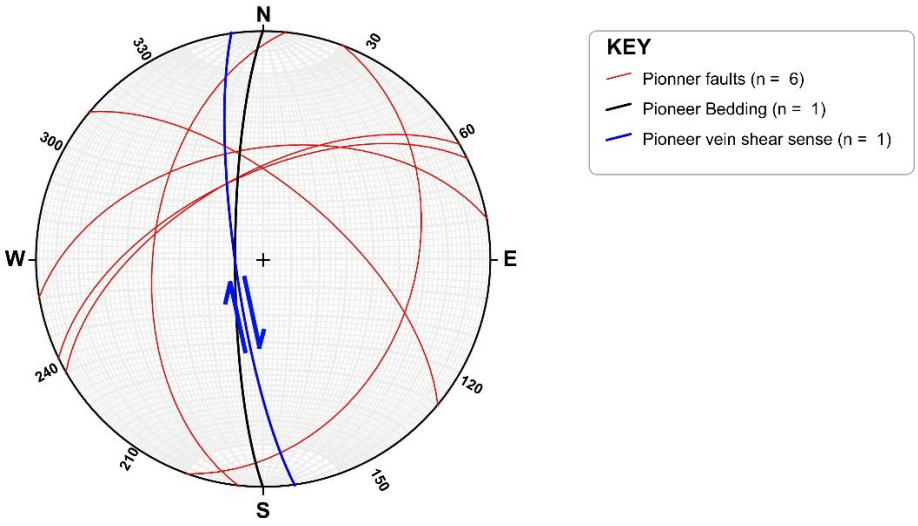

Figure 14: Stereonet of features observed at the PP. The blue plane represents the orientation and sense of movement interpreted from a copper mineralized dilation jog. Note that the orientation of the observed mineralized vein does not follow that of younger faults crosscutting the vein.

Mineralization:

Observed ore mineralization consists of chalcocite with minor disseminated bornite. Gangue mineralization includes quartz, malachite, azurite, calcite, dolomite, pyrite, and ankerite. Notably what makes the PP mineralogically distinct from the other occurrences is its high degree of iron oxidation at surface which is greater then any other observed BVD Cu occurrence. The higher degree of oxidation alongside observed pyrite

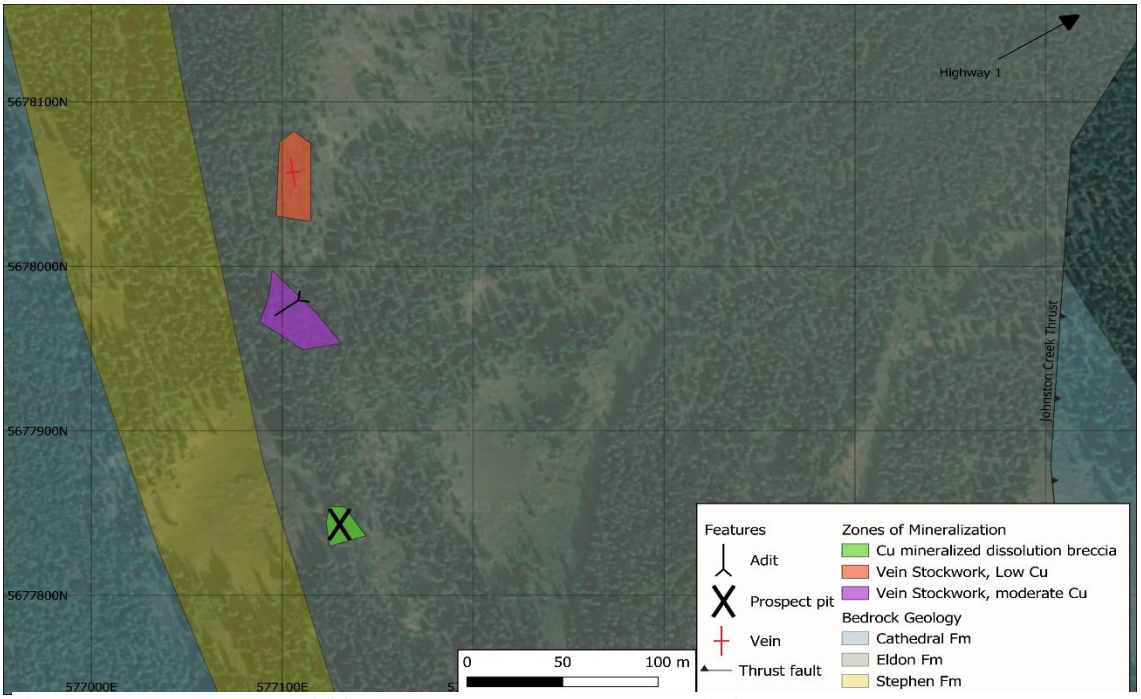

Figure 15: Bedrock geology digitized after Map 1295A. Note the proximity of the Johnston Creek Thrust to the Pioneer prospect.

stringers suggests that this occurrence system maybe more iron rich then the PM or CM. Furthermore, separating the PP from other occurrences is its style of silicification. While both the PM and CM have jasperoid present, the alteration at the PP is coarser grained and associated with pyrite stringers unseen at any other BVD prospect. However, due to the style of mineralization and that the occurrence is hosted within the Eldon Fm, the PP is assumed related to both other Eldon Fm Cu occurrences.

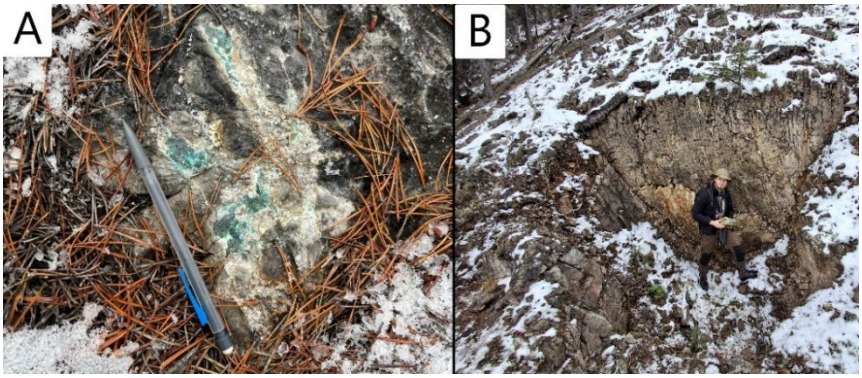

Figure 163: (A) Chalcocite hosted within dilation jog with dextral sense of shear. (B) The Pioneer prospect pit with abundant azurite and malachite mineralization, Matthew Smith posing for scale.

Discussion:

This report, along with prior geological studies of the area concerning metallic mineralization (Evans et al, 1967; Hannigan, 1974) suggest that there are at least three distinct styles of vein-hosted copper mineralization within the BVD. The first and seemingly most frequent type (PM, PP, CM) is the Middle Cambrian massive carbonate hosted quartz vein-copper with evidence of significant supergene enrichment. Silicification is observed at all three observed Middle Cambrian carbonate hosted copper occurrences in the form of jasperoid alteration. Jasperoid altered veins have an similar orientation (after correcting regional folding and faulting) at the CM and PM, suggesting emplacement in similar tectonic regimes prior to major folding, faulting, rotation of bedding within the study area. The similar orientation and spatial association of quartz veins and dissolution breccias observed within the Cathedral and Eldon fms suggests that dissolution breccias associated with MVT mineralization may have acted as conduits for later copper mineralizing fluids and previously created breccia fragments may have assisted as trapping mechanisms for sulphide/copper mineralization. Therefore, due to the similarity between ore mineralization, host rock, and alteration type, there is a likely association between the copper occurrences hosted within Middle Cambrian carbonates and may represent the same ore mineralizing event. Post mineralization faulting at both the PM and the PP, and the restored orientation of veins of CM and PM suggest these copper bearing veins may have been emplaced prior to nearby regional deformation age dated at the nearby Simpson Pass Thrust to be ~161Ma (Pluijm, 2014).

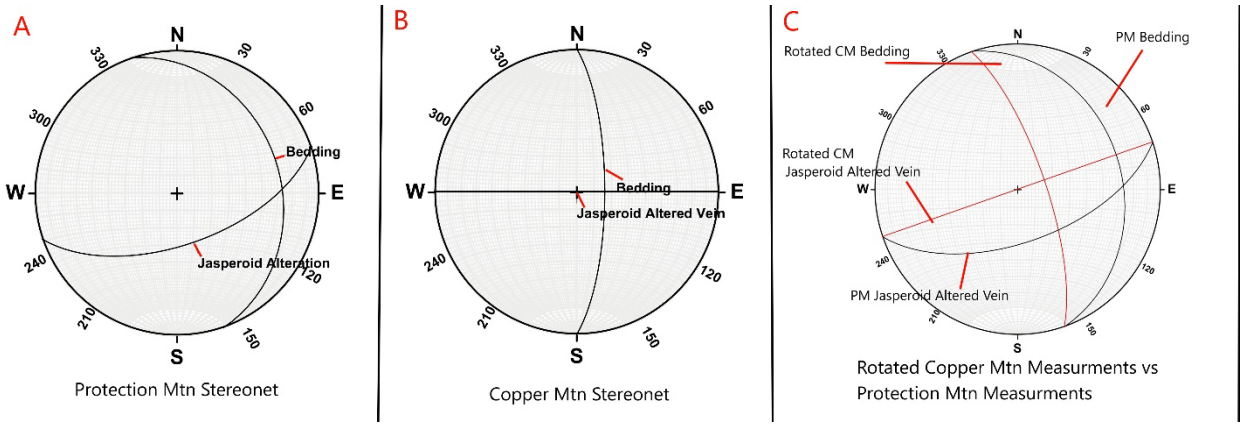

Figure 47: (A) Stereonet of structural features observed at the PM prospect. (B)Stereonet of geological structures observed at the CM. (C) Stereonet of both the PM and CM after the bedding of the CM is rotated to match that of the PM. Note: After the rotation correction of the jasperoid altered veins of both the orientations of the CM and PM prospect nearly perfectly align.

The two other BVD styles of copper mineralization are hosted within the Neoproterozoic Miette Gp. The two styles being the quartz vein hosted copper - zinc veins of the EP (Evans et al, 1967) and the copper – silver calcite veins observed at the PRP. Due to the inability to find the EP at the location described by Evans, 1967 no further description is provided by this report. Comparing and contrasting the two Miette Gp hosted occurrences using prior reports of the EP, the PRP represents an different style of mineralization. The cross-cutting relationships between quartz and calcite veins observed at the PRP suggest that the PRP may have been emplaced later then the EP. Furthermore, the PRP crosscutting relationships with regional foliation fabrics provides the best-known constraint on ore mineralization within the BVD. PRP ore mineralized calcite veins (V2) crosscut both the age dated foliation fabric and unmineralized crenulated quartz veins. However, V2 still retains evidence of deformation implying a late-syn tectonic emplacement. Therefore, due to crosscutting relationships with regional foliation (age dated to ~75Ma (Charlesworth, 1967)) and evidence of compressional deformation influencing ore mineralized veins, the age of mineralization is interpreted to have occurred after 75Ma and before the cessation of compressional deformation in the area ~55Ma (Pluijm, 2014).

Regarding the question of what type of ore deposit BVD copper mineralization falls under. Four main ore deposit models appear applicable to the BVD Cu occurrences are Mississippian – Valley -Type (MVT), Kipushi Cu-Pb-Zn, Polymetallic veins, Mesothermal Base Metal Vein type (Robert J. Fleck, 2002), and Sediment Hosted Cu (Cox, 1992; Fleck, 2002). The process of elimination allows for three of five listed deposit types to be ruled out.

The first deposit model which the BVD does not likely fall under is the MVT model. This is due to the high concentrations of Cu and the low concentrations of Pb-Zn in mineralized veins hosted in both slates and massive carbonates. Mineralization styles and metallic mineral concentrations within the BVD are especially unlike known MVT deposits and prospects in the Canadian Eastern Rocky Mountains such as the Kicking Horse-Monarch Pb-Zn MVT deposits, and the Oldman River and Hawk Creek Prospects. All aforementioned MVT occurrences lack copper mineralization as seen at copper showings within the BVD. Therefore, due to the difference in mineralization type, vein-controlled mineralization, both slate and carbonate host rock make the PRP unlikely to be an MVT deposit. However, the BVD Cu association with some ore forming processes at nearby MVT prospects, especially the effect of traverse basement controlled structural corridors acting as conduits for hydrothermal fluid flow (McMechan, 2012) cannot be ruled out. Especially the Middle Cambrian

hosted Cu occurrences spatially associated with dissolution breccias. Sediment Hosted Cu model can be dismissed due to the lack of red-bed sequences within the study area and the vein hosted nature of BVD copper sulphides unlike the strata bound disseminated copper sulfides typical of sediment hosted Cu models.

BVD Cu occurrences do appear to fall under the umbrella of polymetallic vein type (PVT) deposits. However, the primary characteristic of PVT deposits is a time spatial relationship with igneous sources driving mineralization (Cox, 1992). Within the study area the closest known igneous bodies are the ~1m wide Blackbear Sill (Pana, 2018) and the Ice River Complex respectively located ~17km Northwest and ~30km West of the BVD. The Blackbear sill is hosted by the Miette Gp, its age could not be accurately ascertained (Pana, 2018), while the Ice River Complex has been age dated to 360Ma (Mumford, 2009). The age and distance between the Ice River Complex and the mineralization of the BVD suggests that the Ice River Complex is an unlikely source. The influence of the Miette intrusions could not be fully ruled out. However, their size and distance to the BVD occurrences deems them an unlikely source to metallic mineralization. Note: the Miette Gp host multiple igneous intrusions, notably the Crowfoot Dike which was historically mined for chalcopyrite (Olson, 1994). Despite the lack of a known igneous body driving mineralization, two key points remain which favour an igneous driven system.

The first of which is that within the nearby Toby-Horsethief Creek area there are regarded to be two types of mineralization. Type 1 mineralization is that of MVT or Manto replacement stratiform lead-zinc-silver and Type 2 mineralization consists of discordant vein deposits associated with Late-Cretaceous uplift (Pope, 1990). Metals deposited during Type 2 mineralization are considered the products of remobilization of Type 1 mineralization (Pope, 1990). However, Type 2 mineralization contains significant evidence of primary inputs associated with both quartz monzonitic plutonism and deformation/prograde metamorphism (Pope, 1990). Within the nearby Toby-Horsethief Creek area silver and copper are attributed to Type 2 mineralization due to their normally very low concentrations in Mississippi Valley-type solutions (Edwards, 1986). Furthermore, the second point in favour of an igneous source of metals is the negative Eu/Eu_{N^*} anomaly observed from REEY concentration plots of the PRP ore bearing veins. However, fluid inclusion work is needed to prove that mineralizing fluids precipitated at temperatures lower than 250°C and therefore confirming the Eu/Eu_{N^*} values as accurate indicators of source rock.

The final ore deposit type and possibly the most likely model for the BVD is the solution remobilization and concentration of metals initially deposited and disseminated during the deposition of the Miette Gp. Anomalously high copper concentrations in baseline samples at the PRP chosen for their lack of apparent mineralization may represent syngenetic Proterozoic deposition and dissemination of metallics coherent with the deposition of the Miette Gp. These disseminated metals probably remained mostly undisturbed until the onset of regional metamorphism associated with the Cordillera and Laramide Orogenies. Temperatures sufficient for leaching and remobilization of copper by hydrothermal fluids may be accounted for by residue temperatures estimated of the regional metamorphism ~300°C (Charlesworth, 1967). Fluids carrying metallics leached from the underlaying Proterozoic strata may have then followed conduits of least resistance, such as preexisting paleo faults and dissolution breccias associated with earlier MVT mineralization such as found at the Baker Creek, Copper Mountain, and Pioneer prospects. The high temperature fluids generated from regional metamorphism may represent an mesothermal ore deposit model. Analogous of processes responsible for ore deposition within the BVD could be the Coeur D' Alene, Idaho mesothermal base metal veins. The Coeur D' Alene mesothermal veins have been shown to be the result of solution remobilization product of Pb-Zn disseminated in the Proterozoic strata within the Coeur D' Alene mining district (Fleck, 2002).

Conclusion:

This study leads to the following conclusions:

1) The BVD host unparalleled concentrations of copper-silver mineralization within the Alberta Rocky Mountains.
2) Although still uncertain, ore forming processes responsible for mineralization within the BVD appear to have followed multiple pulses and likely associated with Orogenic processes as shown by petrographic and field observations.
3) The BVD ore forming processes are unlikely to fall under the umbrella of sediment hosted Cu, polymetallic vein, or MVT deposits models, and may represent an mesothermal deposit model.
4) The re discovery of copper mineralization on Panorama Ridge expands on known stratigraphic horizons hosting metallic mineralization within Alberta and British Columbia. The interpreted process concerning the source on controls on metallic mineralization may apply to other mineral showings within the Eastern Rocky Mountains.
5) The Eldon Fm is clearly a favoured stratigraphic unit for further exploration of copper-silver mineralization within and nearby the study area. The controls on mineralization provided by the Eldon Fm are not understood by the authors.
6) Due to the limited scope of this project, further work is recommended by the author to better understand the extent of mineralization and the ore forming processes within the BVD.

Acknowledgements:

We would like to thank the Banff National Park field division for providing the required Collection and Research Permitting, allowing this project to take place. Lab work concerning this project was funded by the Kimberley J Johnston Memorial Fund. We would also like to thank Dr. Chris Collom for his mentorship and assistance in field, and the authors advising professor Dr. Paul Johnston for his mentorship in the field and the stimulating discussions in the field and the office.

We would like to thank Percy Strong for his peer review of this report.

We thank Perry Davis and Clayton Nylund for guiding the authors to historical mine sites and mineral occurrences not marked by the Alberta Geological Survey, and for their in-depth knowledge on the prospecting history throughout Banff National Park.

We would also like to thank Dr. Meg Stewart for her help preparing samples for SEM analysis, although the results were not used in this report. We would also like to thank MRUs geology lab tech Candance Toner for volunteering her time to prepare thin sections. Without her help this project would not have been able to budget for the external work completed during this project

Lastly, we would like to thank my friends and classmates for their help with reconnaissance trips to the study areas of this project and for their input and ideas concerning the work discussed in this report.

References:

Aitken, J. (1971). Control of Lower Paleozoic sedimentary facies by the Kicking Horse Rim, Southern Rocky Mountains, Canada. *Bulletin of Canadian Petroleum Geology*, *19*, 557–569.

Aitken, J. (1997). *Stratigraphy of the Middle Cambrian platformal succession, Southern Rocky Mountains* (Geological Survey of Canada Bulletin 398). Geological Survey of Canada.

Aitken, J. D. (1969). Documentation of the sub-Cambrian unconformity, Rocky Mountains Main Ranges, Alberta. *Canadian Journal of Earth Sciences*, *6*(1), 193–200.

Allan, J. A. (1920). *First annual report on the mineral resources of Alberta*. Edmonton, AB: Government of Alberta.

Bally, A. W. (1966). Structure, seismic data, and orogenic evolution of the southern Canadian Rocky Mountains, British Columbia. *Bulletin of Canadian Petroleum Geology*, *14*, 337–381.

Bernstein, D. P. (1992). Descriptive model of Kipushi Cu-Pb-Zn. In D. P. Cox & D. A. Singer (Eds.), *Mineral deposit models* (U.S. Geological Survey Bulletin 1693, p. 227). U.S. Geological Survey.

Charlesworth, H. A. K., & Warren, J. (1967). *Precambrian geology of the Jasper region, Alberta* (Research Council of Alberta Bulletin 23). Edmonton, AB: Research Council of Alberta.

Cox, D. P. (1992). Descriptive model of polymetallic veins. In D. P. Cox & D. A. Singer (Eds.), *Mineral deposit models* (U.S. Geological Survey Bulletin 1693, p. 125). U.S. Geological Survey.

Cox, D. P., & Singer, D. A. (1992). *Mineral deposit models* (U.S. Geological Survey Bulletin 1693). U.S. Geological Survey.

Dawson, G. M. (1885). *Preliminary report on the geology of the Bow and Belly River region, Northwest Territory*. Geological Survey of Canada.

Debruyne, D., Havel, N., & De Jong, J. (2016). Unraveling rare earth element signatures in hydrothermal carbonate minerals using a source-sink system. *Ore Geology Reviews*, *72*, 232–252.

Dennis, J. S. (1887). *Plan of certain mining claims the property of the Alberta Mining Company in the Bow River Pass, Rocky Mountains, N.W.T.* [Map].

Desjardins, P. R. (2010). *Sedimentology, ichnology and sequence stratigraphy of the Lower Cambrian Gog Group, Southern Rocky Mountains, Canada* (Doctoral dissertation, University of Saskatchewan). University of Saskatchewan.

Edwards, R., & Atkinson, K. (1986). *Ore deposit geology and its influence on exploration*. London, UK: Chapman and Hall.

Evans, T., Campbell, F., & Krouse, H. (1967). A reconnaissance study of some Western Canadian lead-zinc deposits. *Bulletin of Canadian Petroleum Geology*, *15*(4), 257–268.

Evenchick, C. A. (2007). A synthesis of the Jurassic–Cretaceous tectonic evolution of the central and southeastern Canadian Cordillera: Exploring links across the orogen. In J. W. Sears, T. A. Harms, & C. A. Evenchick (Eds.), *Whence the mountains? Inquiries into the evolution of orogenic systems: A volume in honor of Raymond A. Price* (Geological Society of America Special Paper 433, pp. 117–145).

Fermor, P. R., & Miall, A. D. (1992). Tectonics and structure of the Western Canada foreland basin. In R. W. Macqueen & D. A. Leckie (Eds.), *Foreland basins and fold belts* (AAPG Memoir 55, pp. 81–105).

Fleck, R. J., & Edward, R. A. (2002). Age and origin of base and precious metal veins of the Coeur d'Alene Mining District, Idaho. *Economic Geology*, *97*, 23–42.

Hart, E. J. (2021). *Ain't it hell: Bill Peyto's "Mountain Journal"*. Banff, AB: Summerthought Publishing.

Hannigan, K. (1974). *Examination of mineral occurrences in the Southern Rocky Mountains, Alberta and British Columbia*. Alberta Geological Survey.

Kan Li, J., & Bi, J. (2018). Exsolution of chalcopyrite from bornite-digenite solid solution: An example of a fluid-driven back-replacement reaction. *Mineralium Deposita*, *53*(6), 903–908.

Lovering, T. S. (1962). The origin of jasperoid in limestone. *Economic Geology*, *57*(6), 861–889.

McMechan, M. E. (2012). Deep transverse basement structural control of mineral systems in the southeastern Canadian Cordillera. *Canadian Journal of Earth Sciences*, *49*(5), 693–708.

McMechan, M. E. (2022). Structural geometry and kinematic history of the southern Kicking Horse Rim Cambrian carbonate platform: Out-of-sequence thrust faulting in the southern Canadian Rocky Mountains. *Bulletin of Canadian Energy Geoscience*, 69(1), 51–72.

Mickelsen, P., & Schmidt, N. (2021). *2020 geological mapping and sampling of the Vertebrae Ridge Property, near Golden, British Columbia* (BC Geological Survey Assessment Report 39434).

Mumford, T. (2009). *Dykes of the Moose Creek Valley, Ice River Alkaline Complex, Southeastern BC* (Master's thesis, University of New Brunswick). University of New Brunswick.

Olson, R. A., & Desbarats, A. J. (1994). *Regional metallogenic evaluation of Alberta*. Alberta Geological Survey, Alberta Research Council.

Pana, D. R. (2018). *Geochronology of selected igneous rocks in the Alberta Rocky Mountains, with an overview on the age constraints on the host formations* (AER/AGS Open File Report 2018-03). Alberta Energy Regulator.

Pawlowicz, J. G. (2011). *Magmatism and metallic mineralization of the Rocky Mountain fold-and-thrust belt in southwestern Alberta (NTS 82G, H and J): Mineralogy, geochemistry and petrology of selected occurrences*. Alberta Geological Survey, Energy Resources Conservation Board.

Pluijm, B. A. van der. (2014). Orogenic pulses in the Alberta Rocky Mountains: Radiometric dating of major faults and comparison to the regional tectonostratigraphic record. *GSA Bulletin*, *127*(3–4), 480–502.

Pope, A. (1990). *The geology and mineral deposits of the Toby–Horsethief Creek map area, Northern Purcell Mountains, Southeast British Columbia (82K)*. British Columbia Geological Survey Branch.

Price, R.A, & Cook, D.G, & Aitken, J.D, & Mountjoy, E.W. (1975). Geology Lake Louise (East Half) West of Fifth Meridian Alberta- British Columbia, 1:50000 Geological Map, Geological Survey of Canada, Map 1482A.

Price, R.A, & Mountjoy, E.W, & Cook, D.G. (1978). Geology Mount Good Sir (East Half) West of Fifth Meridian British Columbia -Alberta, 1:50000 Geological Map. Geological Survey of Canada, Map 1476A.

Price, R.A, & Mountjoy, E.W. (1972). Geology Mount Eisenhower (West Half) West of Fifth Meridian Alberta, 1:50000 Geological Map. Geological Survey of Canada, Map 1297A.

Price., R.A, & Mountjoy, E.W. (1972). Geology Banff (West Half) West of Fifth Meridian Alberta -British Columbia, 1:50000 Geological Map. Geological Survey of Canada, Map1295A.

Price, R. A. (1981). The Cordilleran foreland thrust and fold belt in the southern Canadian Rocky Mountains. In K. R. McClay & N. J. Price (Eds.), *Thrust and nappe tectonics* (pp. 427–448). Geological Society of London.

Price, R. A., & Fermor, P. R. (1985). Structural section of the Cordilleran foreland thrust and fold belt west of Calgary, Alberta. *Geological Survey of Canada Paper*, *84-114*, 1–16.

Roebuck, L. J. (1978). *Minerals of Alberta*. Edmonton, AB: Hallamshire Publishers.

Rukhlov, A. S. (2011). *Review of metallic mineralization in Alberta with emphasis on gold potential*. Alberta Geological Survey.

Singer, D. A. (1992). *Mineral deposit models* (U.S. Geological Survey Bulletin 1693). U.S. Geological Survey.

Slind, O. L., & Glass, D. J. (2025). Middle Cambrian to Lower Ordovician strata. In G. Mossop (Ed.), *Geological atlas of the Western Canadian sedimentary basin* (Chapter 8). Canadian Society of Petroleum Geologists and Alberta Research Council. https://ags.aer.ca/publications/atlas-western-canada-sedimentary-basin/chapters/chapter-8-middle-cambrian-lower

Taerum, R. T. (2022). Evidence for pre-Cenozoic extension in the eastern Main Ranges of the southern Canadian Rockies. *Geosphere*, *18*(3), 1152–1176.

Timmins, C. (2023, October 6). *Pegasus Resources commences ground program at Golden Project in Southeastern B.C.* Pegasus

Analyte Symbol	Unit Symbol	PM-01-24-GJ	PM-05-24-GJ	PM-06-24-GJ	PM-02-24-MS	PM-03-24-MS	PM-04-24-MS	PM-05-24-MS	PM-18-24-MS	CM-05-24-MS
MgO	%					20.93				
Au	ppb	< 2	< 2	< 2	< 2	< 2	< 2	< 2	< 2	**< 2**
Ag	ppm	0.09	< 0.05	< 0.05	0.24	< 0.05	< 0.05	0.06	2.76	**0.5**
Cu	ppm	2520	99	1620	> 10000	127	1960	> 10000	> 10000	**3830**
Cd	ppm	0.1	< 0.1	< 0.1	0.3	0.4	< 0.1	1.3	< 0.1	**< 0.1**
Mo	ppm	1.68	0.32	0.67	3.75	0.38	0.98	2.55	13.2	**3.39**
Pb	ppm	14.1	1.6	0.5	59.4	0.5	1.9	49.9	47.7	**37.5**
Ni	ppm	1.6	< 0.5	< 0.5	6.1	< 0.5	1.4	9.2	22.5	**8.4**
Zn	ppm	86.3	12.2	33.2	385	9	12.8	1520	1580	**8.3**
S										
Al										
As	ppm	260	10.5	13.3	76.8	28.1	82.1	99.4	224	**132**
Ba	ppm	4	4	2	14	2	2	1	27	**2**
Be	ppm	0.1	< 0.1	< 0.1	< 0.1	< 0.1	< 0.1	< 0.1	< 0.1	**< 0.1**
Bi	ppm	0.06	< 0.02	0.04	0.76	< 0.02	0.03	0.16	1.33	**0.14**
Br	ppm	2.6	0.9	2.7	3.1	6.1	< 0.5	0.9	3.3	**4.1**
Ca	%	2.19	14.4	17.9	1.93	23.1	2.99	0.11	0.11	**0.19**
Co	ppm	1.5	0.5	0.3	4.2	0.3	0.4	2.4	5.3	**7.4**
Cr	ppm	20	< 2	4	< 2	< 2	11	20	< 2	**31**
Cs	ppm	< 0.05	< 0.05	< 0.05	< 0.05	< 0.05	< 0.05	< 0.05	< 0.05	**< 0.05**
Eu										
Fe	%	0.72	0.25	0.39	5.14	0.33	0.9	1.57	15.4	**3.69**
Hf	ppm	< 1	< 1	< 1	< 1	< 1	< 1	< 1	< 1	**< 1**
Ga	ppm	0.4	0.3	0.2	0.9	0.3	1	3.3	1	**0.7**
Ge	ppm	0.2	< 0.1	< 0.1	0.3	< 0.1	< 0.1	0.2	1.6	**0.3**
Hg	ppm	1	< 1	< 1	2	< 1	< 1	11	5	**< 1**
In	ppm	< 0.1	< 0.1	< 0.1	0.5	< 0.1	< 0.1	1.1	1.4	**< 0.1**
Ir										
K	%	0.04	0.03	0.01	0.06	0.02	0.01	0.02	0.03	**0.09**
Li	ppm	9.4	7.1	6.4	5.2	< 0.5	3.6	6.5	1.3	**2.6**
Mg	%	1.15	0.12	1	1	> 10.0	0.69	0.05	0.05	**0.07**
Mn										
Nb	ppm	0.2	0.1	0.2	0.3	0.1	0.7	0.3	0.3	**0.6**
Na	%	0.03	0.03	< 0.01	0.02	0.01	< 0.01	0.01	0.05	**0.02**
P										
Rb	ppm	0.7	0.7	0.3	1.1	0.5	0.3	0.4	0.8	**1.6**
Re	ppm	< 0.001	< 0.001	< 0.001	< 0.001	< 0.001	< 0.001	< 0.001	< 0.001	**< 0.001**
Sb	ppm	9.8	0.4	0.1	0.5	1	0.4	3.3	3.1	**1.1**
Sc	ppm	< 0.1	< 0.1	< 0.1	0.4	0.2	< 0.1	< 0.1	0.6	**< 0.1**

Se	ppm	< 0.1	< 0.1	< 0.1	1.9	< 0.1	< 0.1	0.4	10.9	**0.6**
Sn	ppm	< 1	< 1	< 1	19	< 1	1	2	91	**1**
Sr	ppm	7.6	31.4	36	6.3	28.9	7.4	1.3	16.8	**3.5**
Ta	ppm	< 0.1	< 0.1	< 0.1	< 0.1	< 0.1	< 0.1	< 0.1	< 0.1	**< 0.1**
Te	ppm	< 0.1	< 0.1	< 0.1	< 0.1	< 0.1	< 0.1	< 0.1	< 0.1	**< 0.1**
Tb										
Ti										
Th	ppm	0.1	< 0.1	< 0.1	0.1	0.1	< 0.1	< 0.1	< 0.1	**< 0.1**
Tl	ppm	< 0.05	< 0.05	< 0.05	< 0.05	< 0.05	< 0.05	< 0.05	0.05	**< 0.05**
V	ppm	< 1	< 1	< 1	1	1	< 1	< 1	1	**1**
U	ppm	1	1.7	11.9	3.6	0.3	0.4	2.2	33.2	**< 0.1**
W	ppm	< 1	< 1	< 1	6	< 1	< 1	2	< 1	**< 1**
Y	ppm	0.8	0.9	1.8	1.3	2.7	0.4	0.4	0.3	**0.1**
Zr	ppm	1	< 1	< 1	2	2	< 1	< 1	2	**1**
La	ppm	1	0.4	0.3	3	3.2	0.2	0.2	0.5	**0.4**
La										
Ce	ppm	1.6	1	0.8	5.1	6.2	0.5	0.3	0.7	**0.6**
Ce										
Pr	ppm	0.2	0.2	0.2	0.5	0.7	< 0.1	< 0.1	< 0.1	**< 0.1**
Nd	ppm	0.7	0.7	1.1	1.9	2.3	0.3	0.2	0.2	**0.2**
Nd										
Sm	ppm	0.4	0.3	0.4	0.5	0.4	< 0.1	0.2	< 0.1	**< 0.1**
Sm										
Eu	ppm	0.07	0.06	0.13	0.09	0.12	< 0.05	< 0.05	< 0.05	**< 0.05**
Gd	ppm	0.3	0.3	0.7	0.5	0.6	0.2	0.2	< 0.1	**< 0.1**
Dy	ppm	0.2	0.2	0.4	0.4	0.5	< 0.1	0.2	< 0.1	**< 0.1**
Tb	ppm	< 0.1	< 0.1	< 0.1	< 0.1	0.1	< 0.1	< 0.1	< 0.1	**< 0.1**
Ho	ppm	< 0.1	< 0.1	< 0.1	< 0.1	0.1	< 0.1	< 0.1	< 0.1	**< 0.1**
Er	ppm	< 0.1	< 0.1	0.2	0.1	0.3	< 0.1	< 0.1	< 0.1	**< 0.1**
Tm	ppm	< 0.1	< 0.1	< 0.1	< 0.1	< 0.1	< 0.1	< 0.1	< 0.1	**< 0.1**
Yb	ppm	< 0.1	< 0.1	0.1	0.1	0.2	< 0.1	< 0.1	< 0.1	**< 0.1**
Yb										
Lu	ppm	< 0.1	< 0.1	< 0.1	< 0.1	< 0.1	< 0.1	< 0.1	< 0.1	**< 0.1**
Lu										
Mass	**g**	**1.54**	**1.22**	**1.65**	**1.75**	**1.59**	**1.32**	**1.63**	**0.503**	**1.69**

Analyte Symbol	Unit Symbol	Detection Limit	Analysis Method	Ed-5-1-24-GJ	Ed-4-2-24-GJ	Ed-4-3-24-GJ	Ed-3-24-GJ	Ed-4-24-GJ
Au	ppb	2	INAA	< 2	< 2	< 2	< 2	< 2
Ag	ppm	0.05	MULT INAA/TD-ICP/TD-MS	61	0.41	1.36	136	0.12
Cu	ppm	0.2	MULT TD-ICP/TD-ICP-MS	> 10000	809	3060	> 10000	204
Cd	ppm	0.1	MULT TD-ICP/TD-ICP-MS	0.4	0.2	< 0.1	0.6	0.2
Mo	ppm	0.2	TD-MS	5.4	0.2	< 0.2	25.2	0.7
Pb	ppm	0.5	MULT TD-ICP/TD-ICP-MS	58.4	35.5	25.2	59.3	38.4
Ni	ppm	0.5	MULT INAA/TD-ICP/TD-MS	14.4	42.3	59.2	7.2	2.3
Zn	ppm	0.5	MULT INAA/TD-ICP/TD-MS	61	< 0.5	147	38	< 0.5
S	%	0.01	TD-ICP	3.41	0.14	0.04	2.62	0.21
Al	%	0.01	TD-ICP	2.11	7.83	9.51	1.04	0.45
As	ppm	0.5	INAA	3.7	3.4	0.6	5.6	< 0.5
Ba	ppm	1	MULT INAA/TD-ICP-MS	51600	6720	1340	37300	8240
Be	ppm	0.1	MULT TD-ICP/TD-ICP-MS	0.4	2.2	3.2	0.2	0.1
Bi	ppm	0.1	MULT TD-ICP/TD-ICP-MS	14.3	0.5	1.2	15.9	< 0.1
Br	ppm	0.5	INAA	< 0.5	< 0.5	< 0.5	< 0.5	< 0.5
Ca	%	0.01	TD-ICP	12.5	3.77	0.97	10.3	5.67
Co	ppm	0.1	MULT INAA/TD-ICP-MS	8.8	22.3	32.7	5	1.2
Cr	ppm	1	MULT INAA/TD-ICP-MS	40	84	140	12	10
Cs	ppm	0.05	MULT INAA/TD-ICP-MS	0.53	3.72	5.1	0.39	0.2
Eu	ppm	0.2	INAA	0.6	< 0.2	2.4	0.3	< 0.2
Fe	%	0.01	INAA	1.8	4.39	4.49	1.66	0.68
Hf	ppm	0.1	MULT INAA/TD-ICP-MS	1.2	3.9	4.7	0.5	0.2
Ga	ppm	0.1	TD-MS	5.4	< 0.1	27.5	3.2	< 0.1
Ge	ppm	0.1	TD-MS	< 0.1	0.2	0.2	< 0.1	< 0.1
Hg	ppm	1	INAA	< 1	< 1	< 1	< 1	< 1
In	ppm	0.1	TD-MS	< 0.1	< 0.1	< 0.1	< 0.1	< 0.1
Ir	ppb	5	INAA	< 5	< 5	< 5	< 5	< 5
K	%	0.01	TD-ICP	0.27	2.33	2.83	0.16	0.1
Li	ppm	1	TD-ICP	34	64	91	19	5
Mg	%	0.01	TD-ICP	1.39	1.87	2.11	1.24	0.13
Mn	ppm	1	TD-ICP	6170	2340	888	7410	1390
Nb	ppm	0.1	TD-MS	4.2	2.8	1.6	2.2	1.1
Na	%	0.01	INAA	0.76	1.75	1.98	0.34	0.18
P	%	0.001	TD-ICP	0.05	0.072	0.098	0.055	0.005
Rb	ppm	0.2	MULT INAA/TD-ICP-MS	16.8	138	119	10.6	5.7

Re	ppm	0.001	TD-MS	< 0.001	< 0.001	< 0.001	< 0.001	< 0.001
Sb	ppm	0.1	INAA	< 0.1	0.1	< 0.1	0.4	0.1
Sc	ppm	0.1	INAA	4.9	14.1	17.4	3.7	1.6
Se	ppm	0.1	MULT INAA/TD-ICP-MS	2.5	< 0.1	0.1	2.1	< 0.1
Sn	ppm	1	TD-MS	< 1	2	3	< 1	< 1
Sr	ppm	0.2	TD-MS	> 1000	303	56.9	409	386
Ta	ppm	0.1	MULT INAA/TD-ICP-MS	0.3	< 0.1	< 0.1	0.2	< 0.1
Te	ppm	0.1	TD-MS	0.1	< 0.1	< 0.1	< 0.1	< 0.1
Tb	ppm	0.5	INAA	< 0.5	< 0.5	< 0.5	< 0.5	1
Ti	%	0.01	TD-ICP	0.1	0.34	0.36	0.05	0.02
Th	ppm	0.1	MULT INAA/TD-ICP-MS	7.9	31.3	38.3	2	2.3
Tl	ppm	0.05	TD-MS	0.09	0.76	0.99	0.08	0.15
V	ppm	2	TD-ICP	20	66	85	18	4
U	ppm	0.1	MULT INAA/TD-ICP-MS	3.5	4.1	4.4	4	0.4
W	ppm	1	INAA	< 1	< 1	< 1	< 1	< 1
Y	ppm	0.1	TD-MS	20.9	24	25.1	15.8	13
Zr	ppm	1	TD-MS	43	131	163	18	6
La	ppm	0.1	TD-MS	10.9	62.9	83.2	5.7	3.6
La	ppm	0.5	INAA	19.8	62.3	83.9	11.2	3.9
Ce	ppm	0.1	TD-MS	31.2	136	182	19	7.8
Ce	ppm	3	INAA	38	121	164	25	10
Pr	ppm	0.1	TD-MS	4.3	15.9	20.4	2.8	1
Nd	ppm	0.1	TD-MS	18	57.2	73.4	11.8	4.4
Nd	ppm	5	INAA	47	53	30	9	7
Sm	ppm	0.1	TD-MS	4.2	10.8	11.9	3.4	1.4
Sm	ppm	0.1	INAA	6.9	12.7	15.7	5.7	1.6
Eu	ppm	0.05	TD-MS	0.83	1.5	1.72	0.65	0.33
Gd	ppm	0.1	TD-MS	4.5	7.5	8.8	3.6	1.9
Dy	ppm	0.1	TD-MS	3.5	5.1	5	2.7	2.4
Tb	ppm	0.1	TD-MS	0.7	1	1.1	0.5	0.4
Ho	ppm	0.1	TD-MS	0.6	0.9	1	0.5	0.4
Er	ppm	0.1	TD-MS	1.6	2.5	2.9	1.1	1.1
Tm	ppm	0.1	TD-MS	0.2	0.4	0.4	0.1	0.1
Yb	ppm	0.1	TD-MS	1.3	2.6	2.9	0.8	0.9
Yb	ppm	0.2	INAA	2	3.7	4.3	1.8	0.8
Lu	ppm	0.1	TD-MS	0.2	0.4	0.4	0.1	0.1
Lu	ppm	0.05	INAA	0.11	0.7	0.84	0.06	0.07
Mass	g		INAA	1.87	1.35	1.35	1.82	1.69